JOURNAL OF STRUCTURAL GEOLOGY

Mechanical stratigraphy as a factor controlling the development of a sandbox transfer zone: a three-dimensional analysis

Antonio Ravaglia[a,*], Claudio Turrini[b], Silvio Seno[a]

[a]3D Modelling Laboratory, Dipartimento di Scienze della Terra, Università di Pavia, Via Ferrata, 1, 27100 Pavia, Italy
[b]Total, 2 Place de La Coupole, 92078 Paris La Defense, France

Abstract

In thrust belts, fold–fault terminations are common features of the structural architecture and can pose complicated problems to unravel, in particular when two or more terminations are in close proximity. Such terminations usually reflect pre-existing attributes. Amongst the many factors, lateral variations in the mechanical stratigraphy can control along-strike geometry and kinematics of fault-related folds.

A displacement transfer zone was produced in a compressional sandbox model by means of two adjacent, mechanically different stratigraphic domains. The experiment allowed two discrete chains to develop in the different domains, so that a complex structural setting occurred in the connecting area. Periclinal folds, oblique thrust fronts and oblique ramps developed in the resulting transfer zone. The interaction between periclines in the transfer zone produced lateral culminations in the folded structures. The analysis of displacement across the structural domains revealed that a significant loss of slip along the faults occurred in the relay zone. In this area, imbricate faulting was partially replaced by layer-parallel shortening. A linear relationship appears to exist between the bed length of the thrust sheet and the related fault slip.
© 2004 Elsevier Ltd. All rights reserved.

1. Introduction

Displacement transfer zones are complex structural domains characterized by rapid lateral and vertical changes in the structural elements. In compressional settings, oblique and/or curved thrust fronts, en-échelon plunging anticlines, anastomosing fault patterns, tear faults and lateral ramps are all evidence of transfer zones. Each of these geological structures transfers and accommodates displacement along the strike (Dahlstrom, 1970; Blay et al., 1977; Wilkerson et al., 2002). Where two or more overlapping fault segments occur, the slip across a fault surface decreases and, finally, dies out towards its tip, replaced by the increasing slip on the contiguous fault. Displacement profiles between overlapping structures (Rowan, 1997; Burbank et al., 1999; Nicol et al., 2002) often display loss of slip that may suggest various

mechanisms of shortening accommodations such as folding, faulting and layer parallel shortening. In fact, structures may be the result of the strain accommodated by the arrangement of these three main mechanisms, which mutually act both vertically and laterally. At the thrust tips, whether frontal or lateral, there are localized zones of layer-parallel shortening and layer thickening as well (Coward and Potts, 1983; Geiser, 1988; Butler, 1992). A correct evaluation of the shortening accommodation may improve the cross-section construction and validation process. Besides, the close proximity of more faults and folds poses some questions regarding the geometrical compatibility of the structures in three dimensions. Interference occurs at the lateral tips of faults and folds where the development of low level and generally younger thrusts may cause refolding and strain to occur on the upper and older sheet (Coward and Potts, 1983).

In nature, transfer zones have been widely recognised and greatly studied in different tectonic settings. In fold-and-thrust belts, the role played by the lateral variation of

* Corresponding author. Tel.: +39-0382-505857; fax: +39-0382-505890.
E-mail address: aravaglia@manhattan.unipv.it (A. Ravaglia).

the mechanical stratigraphy is frequently considered one of the most important factors explaining the presence of lateral and oblique ramps, tear faults and pericline terminations (Fischer and Woodward, 1992; Letouzey et al., 1995; Corrado et al., 1998; Philippe et al., 1998; Thomas and Bayona, 2002, among others).

Several physical models have been built to simulate and analyse transfer zones. The induced lateral variations were obtained by imposing:

- variable thickness of the initial stratigraphy (Marshak and Wilkerson, 1992; Marshak et al., 1992; Corrado et al., 1998; Marques and Cobbold, 2002; Soto et al., 2002, 2003);
- vertical passive offset of the basement (Calassou et al., 1993; Corrado et al., 1998);
- horizontal passive offset of the backstop (Calassou et al., 1993);
- variable basal friction (Colletta et al., 1991; Calassou et al., 1993; Cotton and Koyi, 2000; Schreurs et al., 2001; Turrini et al., 2001; Lickorish et al., 2002; Bahroudi and Koyi, 2003; Luián et al., 2003);
- presence of stationary 'foreland' obstacles (Corrado et al., 1998; Turrini et al., 2001; Lickorish et al., 2002; Gomes et al., 2003);
- syntectonic sedimentation or erosion (Barrier et al., 2002; Marques and Cobbold, 2002), and
- non-homogeneous (i.e. interbedded layer composition) mechanical stratigraphy (Corrado et al., 1998; Turrini et al., 2001).

In this work we analyse the influence of mechanical stratigraphy in the construction of a transfer zone and the interactions occurring between faults and folds, while evaluating the complexity of the resulting structural style. We present a detailed analysis of a compressional sandbox model, being part of a set of experiments focusing on transfer zone simulation with lateral variation of the mechanical stratigraphy. We reconstruct the three-dimensional geometry of folds and faults in the resulting transfer zone, giving a relationship between the lateral variation of a thrust sheet and the slip along its fault. Finally, we assess the partitioning of strain both along strike and vertically.

2. The experiment

For a complete historical review of modelling techniques and a complete literature list, see Koyi (1997), Cobbold and Castro (1999), Ranalli (2001) and Schellart (2002). We reproduced a displacement transfer zone by simultaneously deforming two adjacent, mechanically different, stratigraphic domains within a sandbox apparatus (Fig. 1). The first domain was a multilayer (non-homogeneous domain) composed of sand and glass microbeads beds; the second was a sand-only domain (homogeneous domain). The
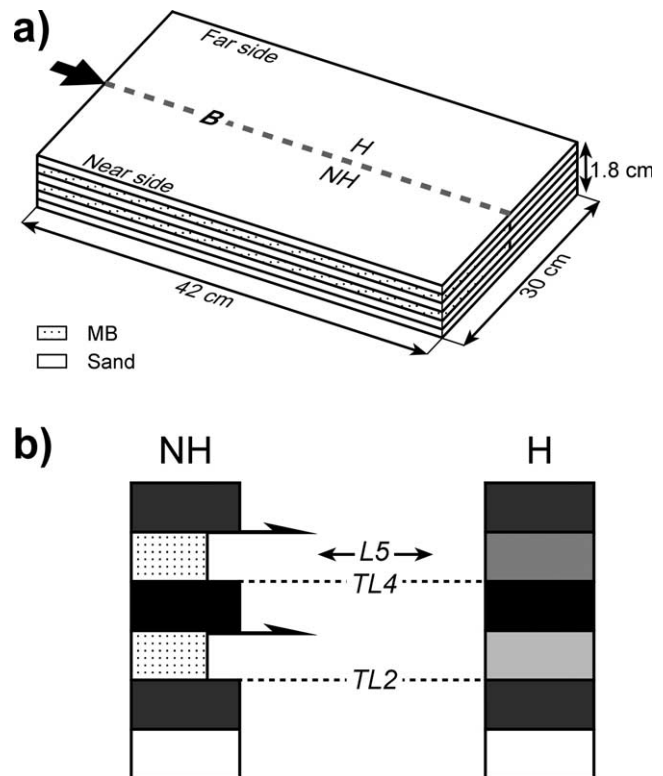

Fig. 1. Initial model configuration. (a) Block diagram of the experimental conditions (not to scale). (b) Sketch of the mechanical stratigraphy of the two domains, with the inter-strata detachment indicated. B = boundary line; H = homogeneous domain; NH = non-homogeneous domain; MB = glass microbeads; TL2 and TL4 = top layers used for measurements; L5 = layer 5.

thickness was constant across the model. The boundary (B) between the two sectors was parallel to the shortening direction and was located along the central part of the model.

The initial model was 42 cm long, 30 cm wide and 1.8 cm high. We used two types of granular materials with different physical parameters: sand, and glass microbeads. The sand has an angle of internal friction (ϕ) of 33° and a grain size of 100–300 μm. In the near side of the model, i.e. from 0 to 15 cm along-strike, two layers of 3 mm each of glass microbeads replaced the sand, at 6 and 12 mm from the base of the model. Glass microbeads are suitable for simulating natural rocks because they enable low basal friction detachment (Sassi et al., 1993) and inter-strata slips (Turrini et al., 2001) to occur. Glass microbeads have $\phi = 24°$, due to their high sphericity and rounding (Schellart, 2000), and a grain size of 300–400 μm. For this reason, in the non-homogeneous domain, ϕ had an average value of 30°. The two domains were shortened over the same basal detachment, this having a friction angle (ϕ) of 32°.

The foreland side of the box was not closed. As soon as sand started falling down from the foreland edge of the box, but only in the far left-hand side (homogeneous domain), the total shortening was 18.5 cm (44%) and the experiment was

considered finished. During the experiment, neither erosion nor sedimentation were simulated. The analysis of 1-cm-spaced sections across the final model, combined with a progressive snap-shot of the evolution in plan, aided the three-dimensional reconstruction of the obtained deformation geometries through time and space. The opportunity to see clear cut-offs allowed the dip length of the thrust sheet and slip along the faults to be measured accurately. Measurements were performed on two stratigraphic levels.

The model transfer zone was analysed by 11 cross-sections, taken every centimetre from 10 to 20 cm from the near side of the sandbox apparatus. The interpreted structures were then measured and contoured to reconstruct the three-dimensional deformation distribution across the modelled transfer zone. Structure contour maps for faults and layering were constructed based on digitized interpretations of cross-sections.

3. Results

Two distinct thrust belts develop in each domain (Figs. 2 and 3). In the non-homogeneous domain, far from the boundary line, first-order thrust sheets develop, along with second-order thrust faults, these being detached over the shallow glass microbeads level (Fig. 4d–g). Conversely, in the homogeneous domain, only first-order thrusts occur. In both the domains, only small backthrusts appear, which are slightly more developed in the homogeneous domain.

The model kinematics follows a generic piggyback sequence, from the hinterland to the foreland, without significant out-of-sequence events. The main feature of the experiment was the alternate development of the four external thrusts (labelled 5–8; Fig. 2) in the two compartments of the model. After the continuous growth of thrusts 3 and 4 over the entire width of the sandbox, thrusts 5–8 developed as related to discontinuous periclinal faulted folds plunging towards the centre of the model. Thrusts 5 and 7 formed in the homogeneous domain, then rapidly propagated laterally with fronts curved towards the middle of the model, and crossed the boundary for a distance of 4.2 cm. Thrust faults 6 and 8 developed in the non-homogeneous domain, then propagated along-strike with oblique fronts across the boundary. Such thrusts extended into the opposite domain only for 2 cm.

3.1. The transfer zone

A 6.2-cm-wide transfer zone parallel to the shortening direction formed in the centre of the model, representing the connection between the homogeneous and non-homogeneous domains. This zone was characterized by the contemporaneous occurrence of all faulted folds. The close-up photograph of the transfer zone in plan view (Fig. 3) reveals a braided pattern of thrust fronts. Thrusts 3 and 4 were almost parallel to the backstop away from the

boundary line and are slightly oblique in the transfer zone. For instance, thrust 4 in the transfer zone is oblique and has an acute angle of 72° with respect to the shortening direction. Thrust faults within the transfer zone tend to form with strike directions oblique (rather than perpendicular) to the shortening direction, and do not tend to rotate during the temporal evolution of the thrust system. The oblique front connects two thrusts, different both in bed length and fault slip. Structures from 5 to 8 are nearly confined to the domain where they grew, and terminate towards the centre of the model with an oblique front. All of the pericline-related thrust surfaces branch from the base of the model and laterally join the adjacent and earlier surface (thrusts 5–8; Figs. 3 and 4).

Fault surfaces in the transfer zone are oblique ramps connecting frontal ramps on both sides (Figs. 5 and 6a). Structural contours of faults 6–8 exhibit the geometry of the oblique ramps that are normally associated with plunging anticlines. The oblique ramp along fault 6 dips at 25° and the angle between the strike of the ramp and the transport direction is 55°. Along fault 7, the oblique ramp is very narrow and similar to a lateral ramp. The oblique ramp dips at 28°, and the angle between the strike of the ramp and the transport direction is 26°. Fault 8 shows a wide oblique ramp dipping at 25°; the angle between the strike of the ramp and the transport direction is 50°. At depth, thrust fault 8 branches off the footwall of the adjacent thrust fault 7 (Fig. 4b). Similarly, thrust surface 6 branches off the footwall of fault 5. The position of the oblique ramps shows that the transfer zone, or the interference area, is more developed in the non-homogeneous domain than in the homogeneous one.

3.2. Thrust sheet geometry

Except for structures in the hinterland, which are continuous throughout the model, the four more external folds are periclines plunging towards the centre of the model (Figs. 3, 6b and 7). The bed lengths of such thrust sheets strongly decrease along-strike, and become zero approaching their tip in the opposite domain (Fig. 8a). In the non-homogeneous domain, thrust sheets have the shape of recumbent thrust related folds (see sheets 6 and 8, Fig. 4d–g), whereas in the homogeneous domain they are upright thrust related folds (see sheets 5 and 7; Fig. 4a–c).

Only in the non-homogeneous domain do two orders of structures develop; first-order faulted folds branch from the basal detachment, and second-order smaller thrust sheets detach over the shallow glass microbeads bed. The second-order structures are poorly developed because of the mutual competition between the two weak layers. Indeed a higher basal friction décollement would have likely produced a greater second-order structures occurrence (Turrini et al., 2001, see their fig. 18). However, second-order thrusts terminate as they approach the homogeneous domain (Figs. 2 and 3).

a) T00

Near side

Far side

NH   B   H

b) T04   10 cm

3
4

c) T06
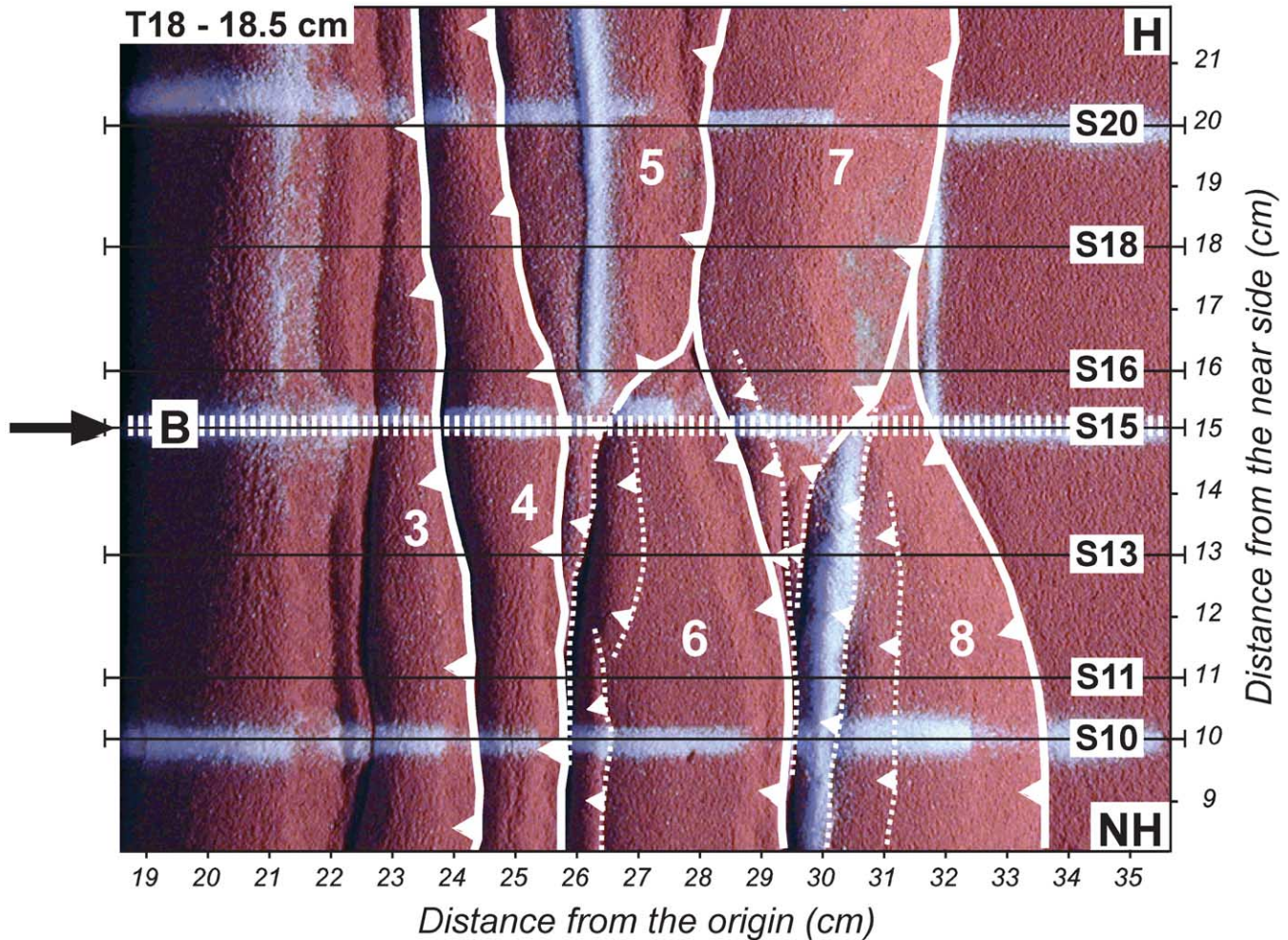
5

d) T07

6

e) T11

7

f) T13

8
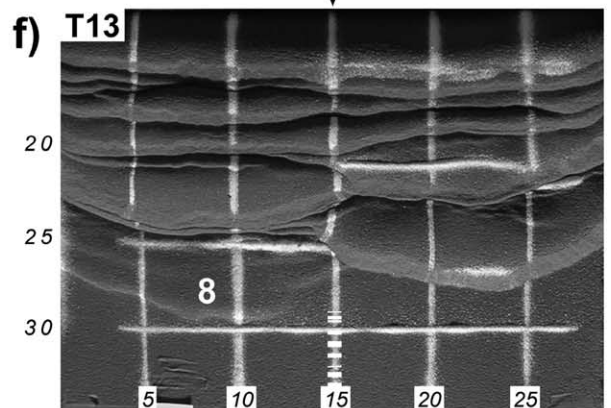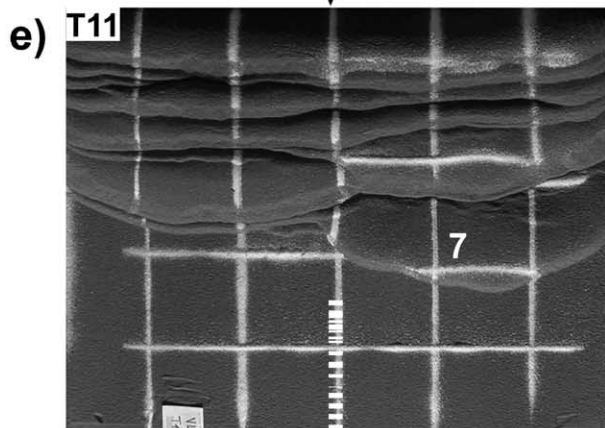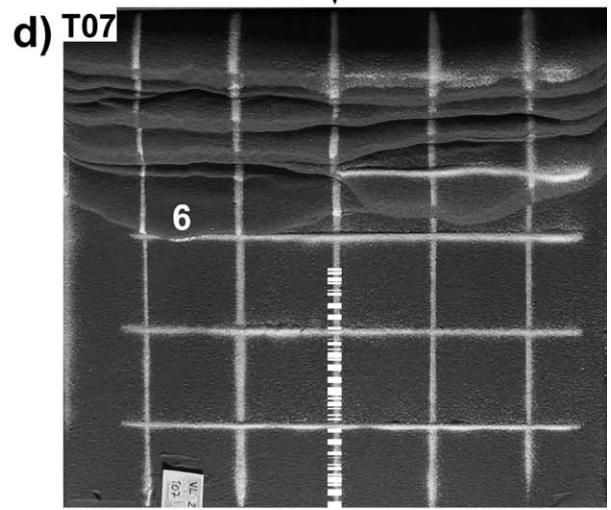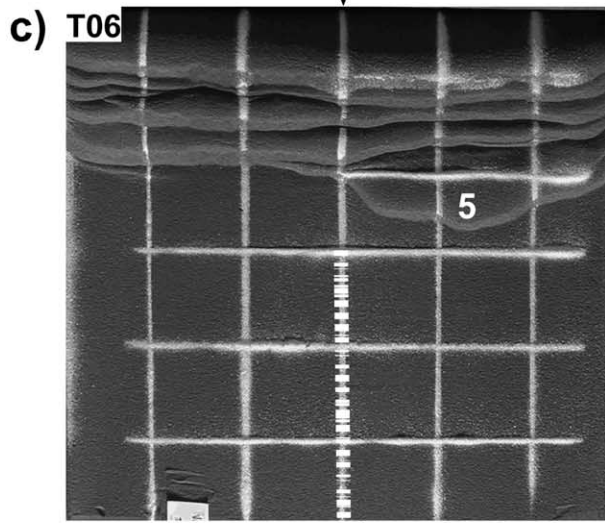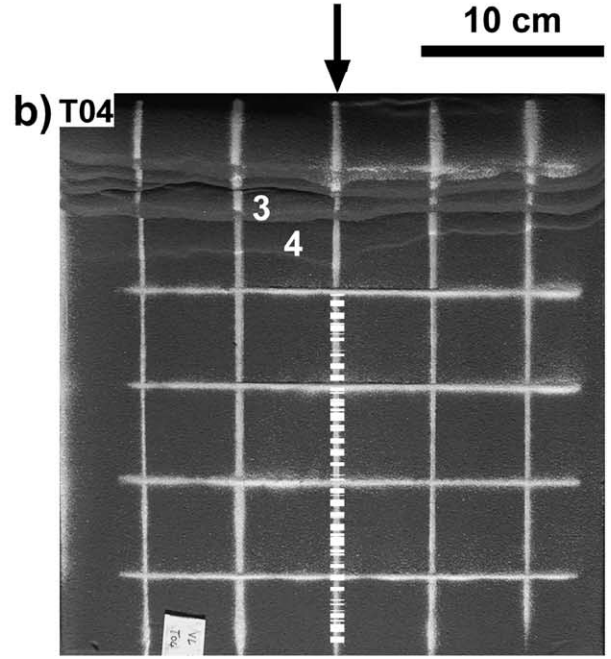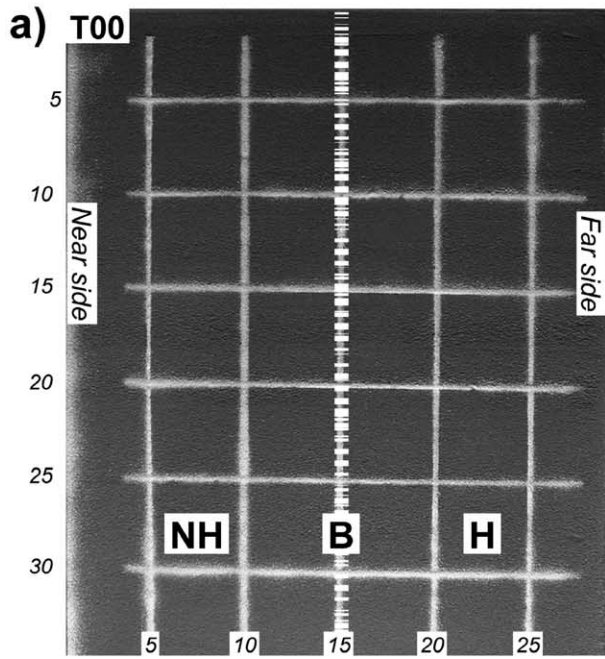
Fig. 3. Detailed map view showing the braided pattern of thrust fronts in the displacement transfer zone at the end of the experiment; traces of seven cross-sections are shown. Dotted lines represent second-order thrust faults. S = cross-section position from the near side, in centimetres. Glass microbeads layers are indicated with arrows. B = boundary line; H = homogeneous domain; NH = non-homogeneous domain.
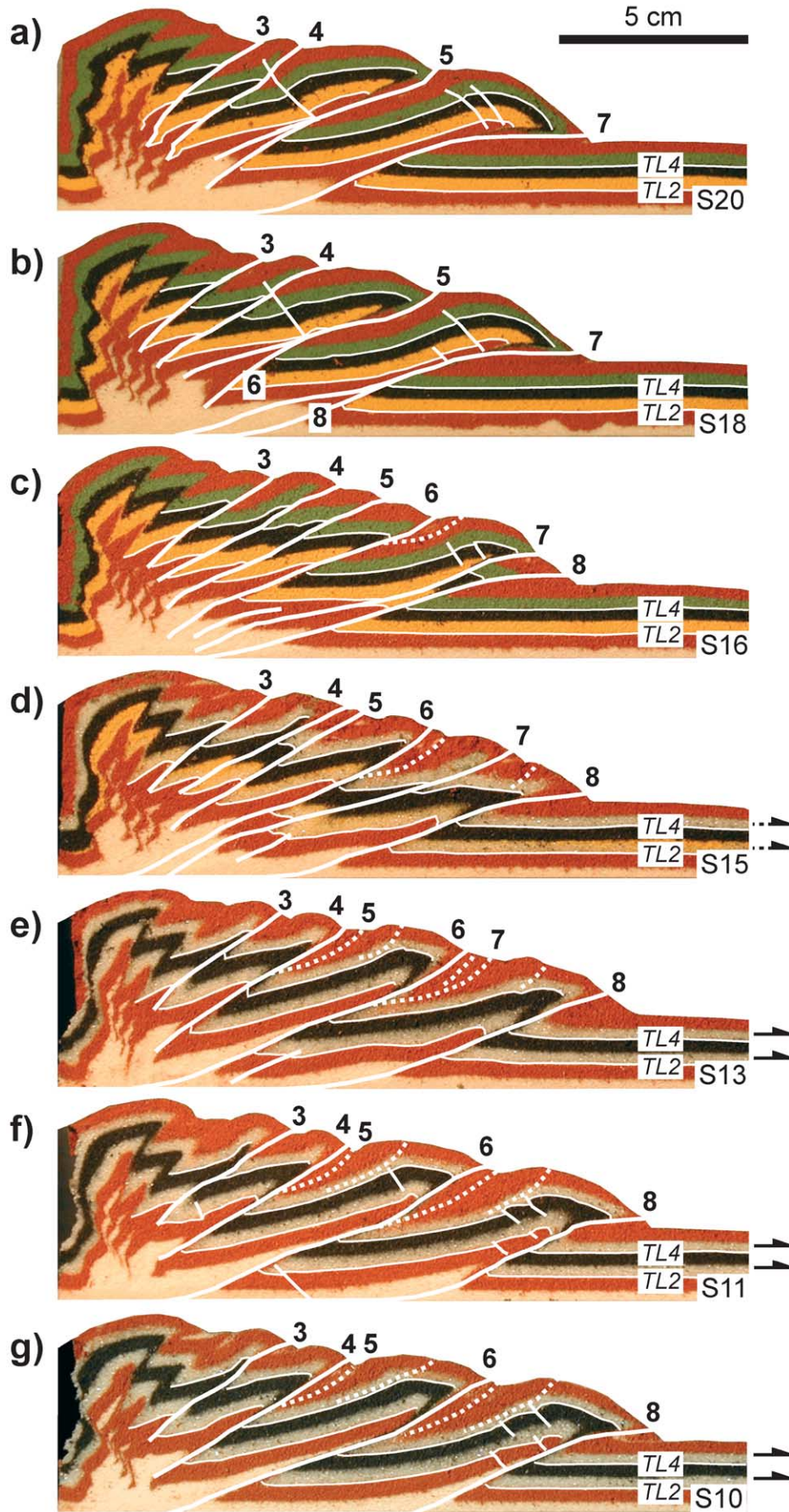
The four external periclines have been individually contoured at the top of layer 4 (labelled TL4 in Figs. 1 and 4). Interference patterns reveal that interplay occurred between different age structures, especially for old thrust sheets; for instance, towards the depression of fold 5 (Figs. 6b and 7a) a subculmination exists, probably due to the uplift of fold 6. Fold 6 is influenced by its lateral and underlying fold 7, and also exhibits a subculmination (Fig. 7b). Folds 7 and 8 do not display any lateral subculminations. Fold 8 reveals a very strong deflection of the main hinge at the end of the experiment (55° with respect to the shortening direction; Fig. 7d) and is parallel to the thrust front. Finally, thrust sheets developed in the non-homogeneous mechanical stratigraphy seem to have a greater bed length (Fig. 8a).

4. Discussion

4.1. Transfer zone arrangement

The model transfer zone is a broad structural domain that develops parallel to the shortening direction. It is characterized by the occurrence of fold terminations, axial plunge and oblique fold hinges. Faults and folds in the transfer zone undergo more than a single phase of deformation. As a result, faults reveal secondary deformation due to uplift (Figs. 5a and 9a), and periclines display lateral subculminations towards their depressions (Fig. 7a and b). The related pericline fault surfaces appear to be physically linked (Fig. 9b). Older folds do not display a clear horizontal deflection of the hinge line, but they seem to maintain their original

Fig. 2. Map view of the deformation kinematics. The dotted line (B) represents the boundary between the two domains. The white square grid is 5 cm. (a) Initial state; (b) after 5 cm of shortening (11.9%); (c) after 8 cm of shortening (19%); (d) after 9 cm of shortening (21.4%); (e) after 13 cm of shortening (31%); (f) after 14.5 cm of shortening (34.5%). B = boundary line; H = homogeneous domain; NH = non-homogeneous domain.

5 cm

a) 3 4 5 7 TL4 TL2 S20

b) 3 4 5 7 6 8 TL4 TL2 S18

c) 3 4 5 6 7 8 TL4 TL2 S16

d) 3 4 5 6 7 8 TL4 TL2 S15

e) 3 4 5 6 7 8 TL4 TL2 S13

f) 3 4 5 6 8 TL4 TL2 S11
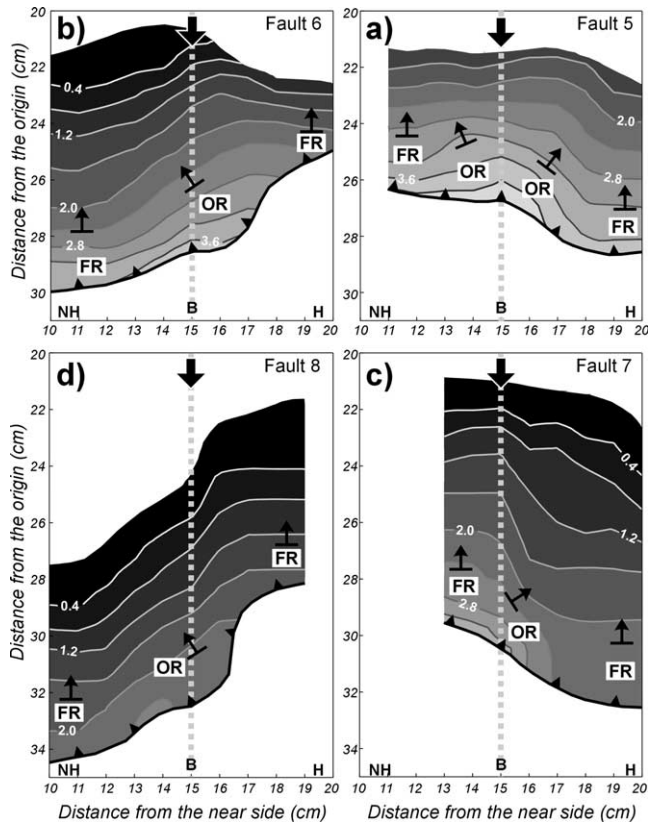
g) 3 4 5 6 8 TL4 TL2 S10

Fig. 5. Contoured fault surfaces. Elevation from the base of the model is in centimetres, the contour interval is 0.2 cm. (a) 5, (b) 6, (c) 7 and (d) 8. FR = frontal ramp; OB = oblique ramp. The dotted line represents the boundary (B) between the non-homogeneous (NH) and the homogeneous (H) domains. Plots are not overlapped.

pattern throughout the entire experiment (compare with Fig. 2).

4.2. Thrust fault displacement

We measured thrust front displacement in plan view along profiles 10, 15 and 20 (Fig. 10) during different steps of the deformation, using the reference grids in the hanging wall and footwall of each thrust. The displacement pattern is similar in the domains far from the boundary line (compare Fig. 10a and c), yet the displacement seems greater in those thrusts developed in the non-homogeneous domain. Such divergence is clearer along the central profile (Fig. 10b); undoubtedly, structures 6 and 8 accommodate larger displacement relative to structures 5 and 7. The mechanical stratigraphy, different in each domain, seems to control the displacement (activity) of thrusts.

We also measured and plotted fault slip in the vertical plane of shortening for each section in the final model. Fault
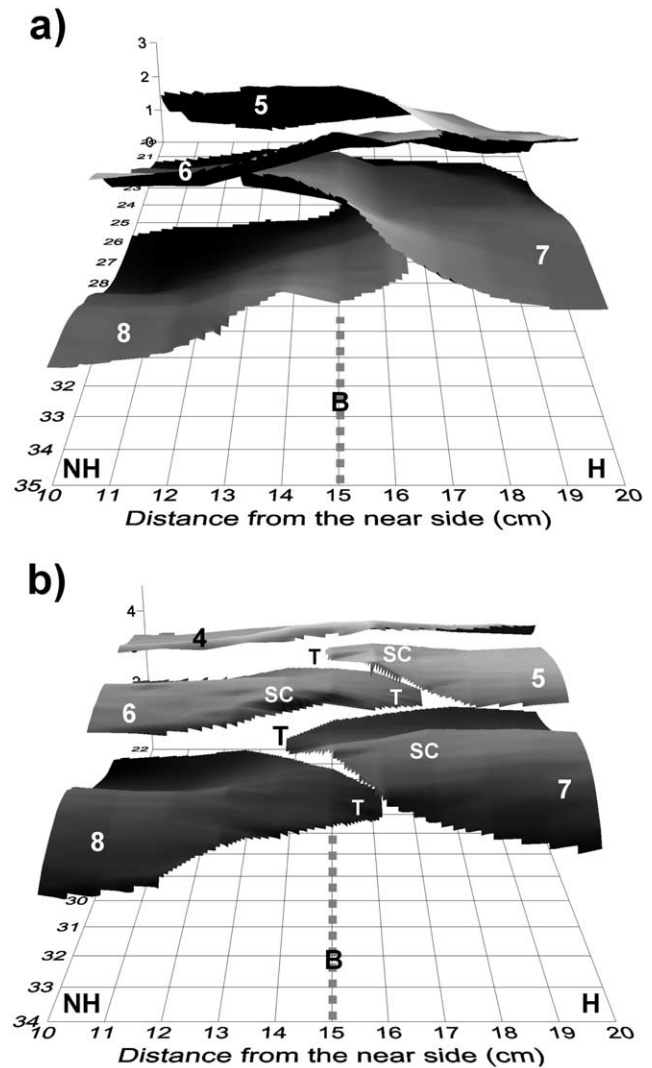

Fig. 6. Three-dimensional visualization of faults (a) and folds (b) in the transfer zone. The dotted line represents the boundary (B) between the non-homogeneous (NH) and the homogeneous (H) domains. SC = lateral sub-culminations; T = lateral terminations.

slip diminishes toward pericline depressions (Fig. 8b): the cumulative amount of slip for all of the faults exhibits a significant loss in the transfer zone: nearly 41% with respect to the 'normal' areas. As for thrust sheet length, slip also seems to be greater in the non-homogeneous than in the homogeneous domain.

From the wedge theory perspective (Davis et al., 1983), the critical taper simplified for a dry cohesionless wedge relies on the friction of the basal décollement (according to a direct relationship) and on the friction of the analogue materials (according to a reverse relationship). In our model, basal friction is the same in both domains ($\phi = 32°$), the

Fig. 4. Seven cross-sections cut in the transfer zone. Dotted lines represent second-order thrust faults. S = cross-section position from the near side, in centimetres. Glass microbeads layers are lightest grey and are indicated with arrows. TL2 and TL4 = top layers used for measurements; B = boundary line; H = homogeneous domain; NH = non-homogeneous domain.
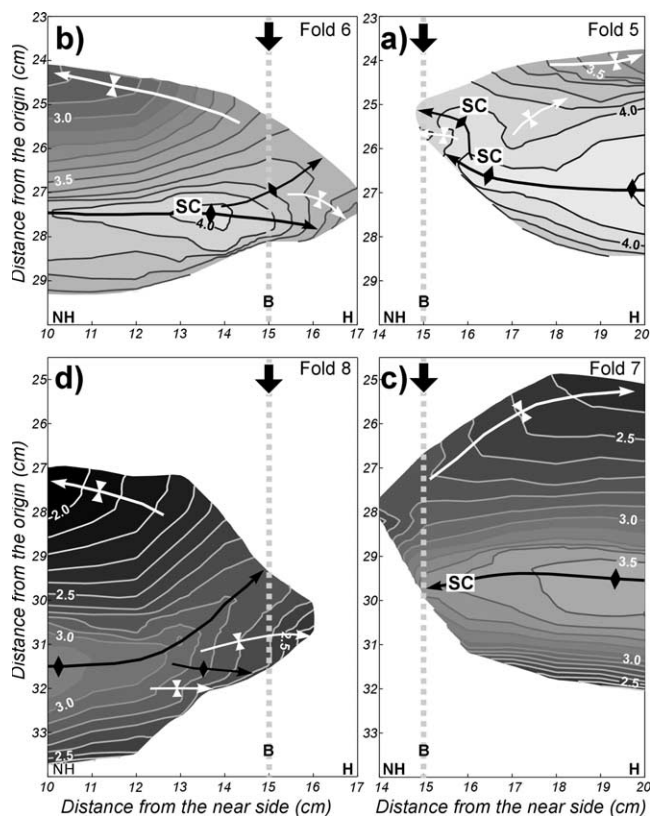
Fig. 7. Contoured fold surfaces, top layer TL4. Elevation from the base of the model is in centimetres, the contour interval is 0.05 cm. (a) 5, (b) 6, (c) 7 and (d) 8. The dotted line represents the boundary (B) between the non-homogeneous (NH) and the homogeneous (H) domains. Plots are not overlapped. SC = sub-culminations.

Fig. 8. Plots of (a) the lateral variation of thrust sheet bed length (*L*) measured along each cross-section; (b) the lateral variation of the slip (*S*) measured along each cross-section; (c) the thrust sheet bed lengths (*L*) against slip (*S*) for each pericline showing a good linear relationship (filled line). Only thrust sheet 8 diverges from this trend due to its younger age (dotted line). Here the regression line has been constructed using thrusts 5–7 as a single series. The layer considered is TL2 of Figs. 1b and 4.

friction angle in the homogeneous domain is $\phi = 33°$ (only sand) whereas in the non-homogeneous domain the use of glass microbeads lowers the average angle of internal friction of the material ($\phi = 30°$). Applying the approximated equation for a dry cohesionless wedge (Liu et al., 1992) and using values of the two domains, we obtain a higher theoretical critical taper in the non-homogeneous domain ($\alpha + \beta \cong 12°$) with respect to the nearby homogeneous domain ($\alpha + \beta \cong 10.6°$), made up of sand solely ($\phi = 33°$). As always, in the analogue experiment, the early steps of deformation involve building up the topographic slope to the critical angle; as a consequence, in both domains the early shortening was absorbed by closely spaced thrust faults. Thus, the critical value was exceeded first in the homogeneous domain because it requires a lower critical taper, and as a result, the deformation shifted forward to produce a longer thrust sheet (thrust 5; Fig. 2c); in contrast, at the same time in the non-homogeneous domain the topographic slope was not high enough to deform the foreland. Once the critical angle was surpassed in the non-homogeneous domain as well, the front of deformation progressed towards the foreland (Fig. 2d).

Fault kinematic analysis involves measurement of the slip of each cut-off using the footwall ramp as a pin (Fig. 11). Slip measu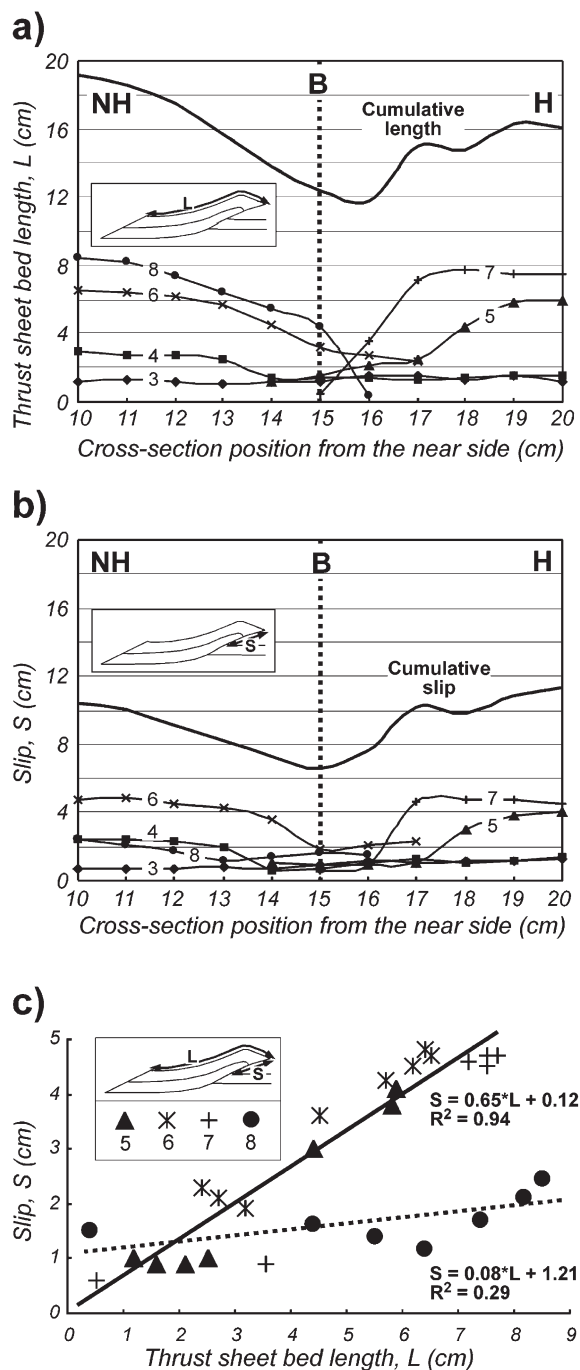res are then contoured and projected onto a vertical plane. The result is a map of the distribution of slip on the fault surface. Such analysis allows improved three-dimensional interpretation of faults and their interrelationship: for instance, it is useful in the investigation of branching areas (Needham et al., 1996). All of the maps
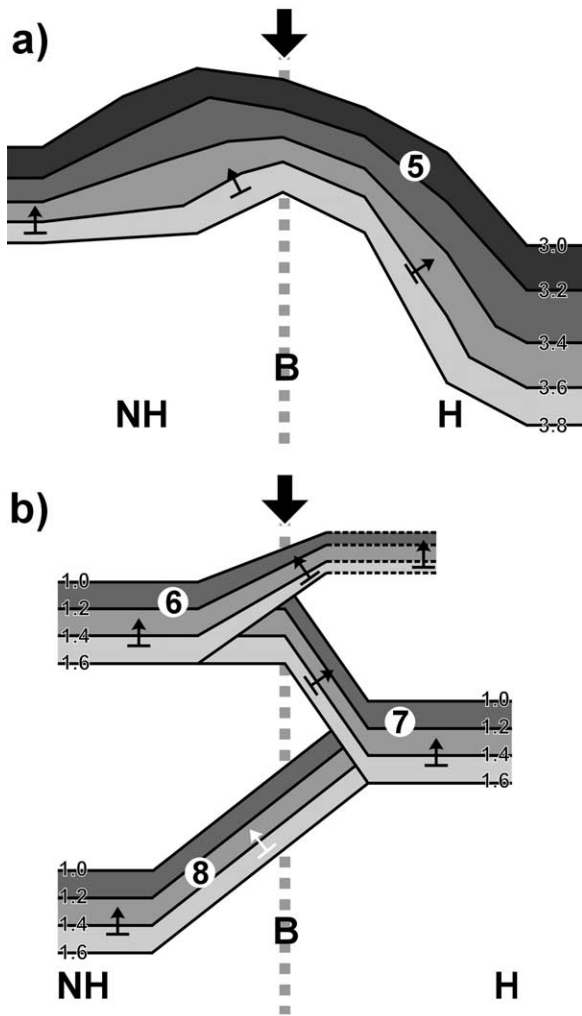
Fig. 9. Simplified contour diagrams. (a) Upwardly curved fault surface 5 due to a second phase of deformation. (b) Hard-linked relationship between pericline fault surfaces 6–8. The greyscale represents the elevations from the base of the model (in centimetres). The dotted line represents the boundary (B) between the non-homogeneous (NH) and the homogeneous (H) domains.
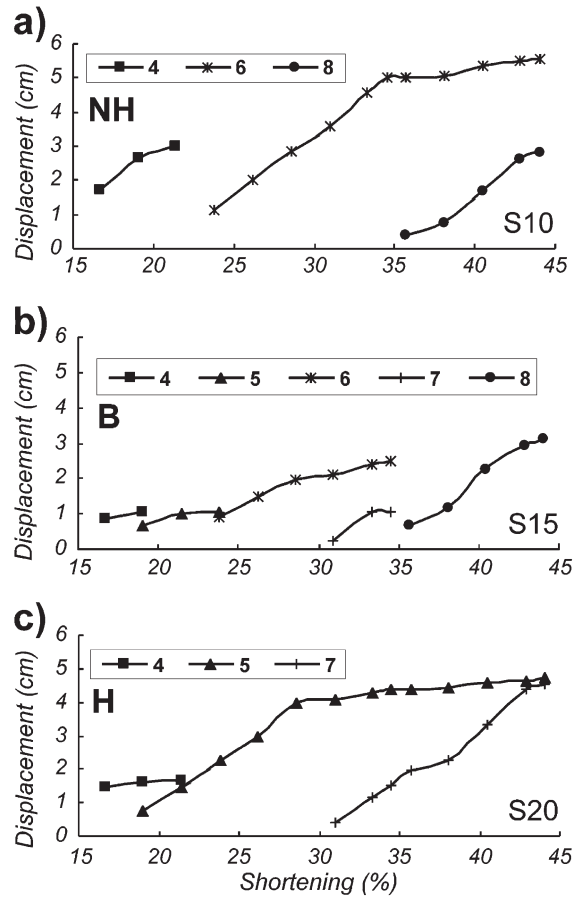

Fig. 10. Displacement diagrams showing the kinematic evolution measured in map view. (a) Thrusts 4, 6 and 8 along profile 10 in the non-homogeneous domain (NH). (b) Thrusts 4–8 along the boundary line (B). (c) Thrusts 4, 5 and 7 along profile 20 in the homogeneous domain (H).

show that slip varies both along strike and along dip. The greatest slip normally occurs nearly in the middle of the stratigraphy and where the thrust front is more advanced (compare Figs. 3 and 11). Faults display a small amount of slip approximately along cross-section 15, which corresponds to the oblique ramps. Fault surfaces in the homogeneous domain (faults 5 and 7; Fig. 11b and d) seem to display a greater lateral gradient of slip than fault surfaces in the non-homogeneous domain (faults 4 and 6; Fig. 11a and c). On every fault surface, the along-strike gradient of slip depicts linkage between two faults.

4.3. Thrust sheet bed length versus slip

As previously shown, thrust sheet bed length and slip along the faults decrease simultaneously towards the pericline depressions (Figs. 8a and b and 11). The plot of thrust sheet bed length against slip, measured on each cross-section (Fig. 8c), displays a good linear relationship and, mainly, a similar coefficient of the regression line for periclines 5–7 (here we consider these three thrusts as a single series, not having appreciable differences). Despite both the slightly greater bed length and map view displacement measured in the non-homogeneous with respect to the homogeneous domain, thrusts are not enough to suggest any general rule in order to distinguish between the two domains. This plot can help to predict the three-dimensional geometry of a 'steady' thrust sheet, provided that either the footwall or hanging wall are known or, in exchange, the slip is determined. Also, it may afford the geologist a test of the activity of a thrust when compared with others of the same belt. The plot shows that slip $S \cong 0.65L$ or, alternatively, thrust sheet bed length $L \cong 1.54S$, at least for this experimental configuration. Only thrust sheet 8 greatly departs from this trend, as its slip is low with respect to its bed length; the slope of the correlation line is shallow and reveals its young age; indeed, this structure was the youngest fault and still active at the end of the experiment.
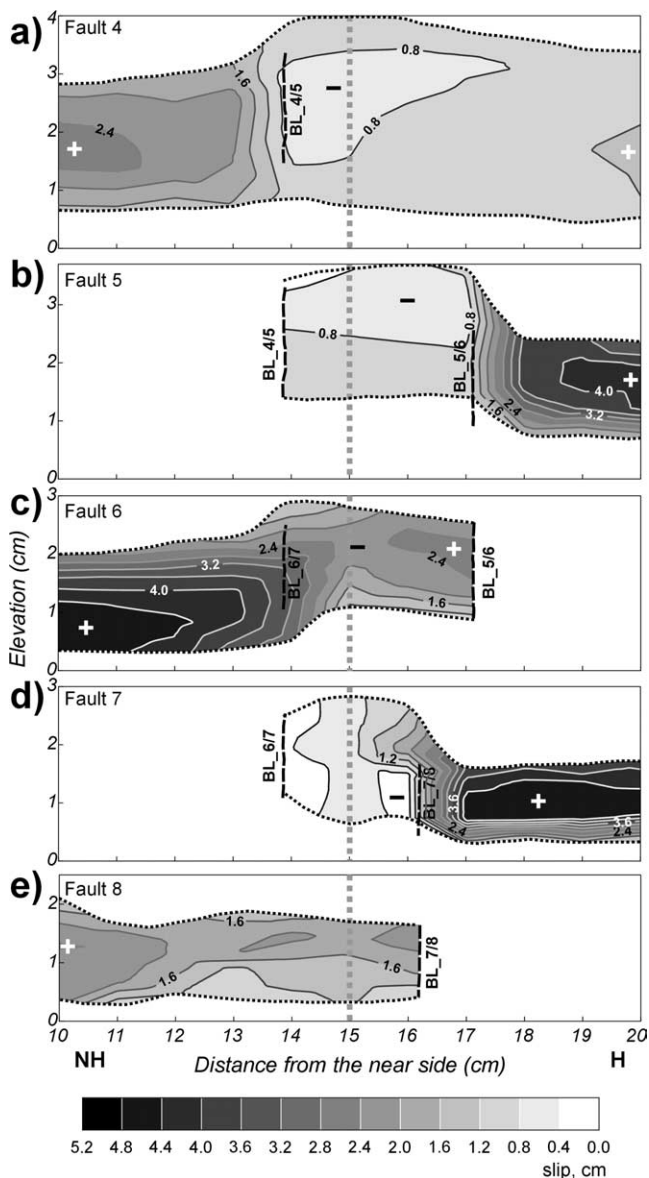
Fig. 11. Maps of the slip on the faults. (a) 4, (b) 5, (c) 6, (d) 7 and (e) 8. Contour interval is 0.4 cm. Black dotted lines represent the lower and upper limits of the footwall cut-offs. Black hatched lines (BL) represent branch lines between faults. Vertical grey dotted lines represent the boundary (B) between the non-homogeneous (NH) and the homogeneous (H) domains.
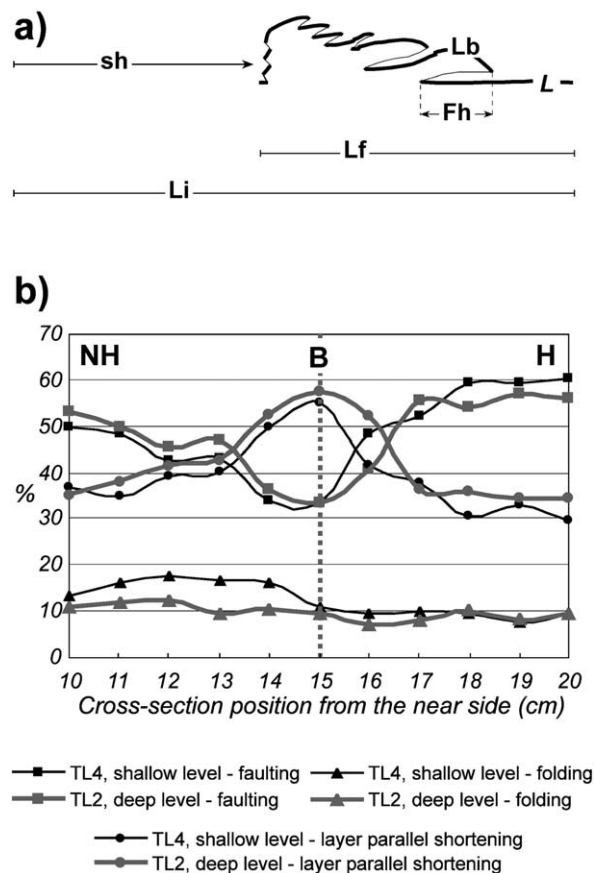

Fig. 12. (a) Bed length balancing method used in this paper. Sh = shortening; Lb = thrust sheet bed length; Fh = fault heave; Lf = final length of the model; Li = initial length of the model; L = layer used as reference. (b) Diagram showing how the strain is partitioned between faulting (squares), folding (triangles), and layer-parallel shortening (circles) for shallow (TL4, black lines) and deep (TL2, grey lines) structural levels. Layer-parallel shortening greatly increases in the transfer zone and replaces the amount of shortening due to faulting.

4.4. Strain partitioning

The loss of slip along the faults (Fig. 8b) reveals that a complicated strain partitioning may occur in the model transfer zone domain. As a consequence, it is necessary to analyse exactly how the strain is accommodated across the transfer zone. The kinematics of layer-parallel shortening has been described in two-dimensional sandbox models (Mulugeta and Koyi, 1992; Koyi, 1995). Assuming that the model deformation can be partitioned into three main mechanisms, i.e. layer-parallel shortening, faulting and folding, we measured bed shortening (Fig. 12a) using the

following methodology (see also Mulugeta and Koyi, 1987):

Input:
Fault heave (Fh);
Thrust sheet bed length (Lb);
Initial length of the model (Li);
Final length of the model (Lf).
Output:
Faulting = (Fh);
Folding = Lb − (Lf + Fh);
Layer-parallel shortening = Li − Lb.

Because we measured the heave as the horizontal distance between cut-offs, and we know that older and internal thrust faults are rotated, we certainly measured a heave value that is less than the actual. Consequently, the calculated amount of folding could be slightly greater than the actual. Further measurements have been done taking into account the vertical rotation of thrust faults. Results
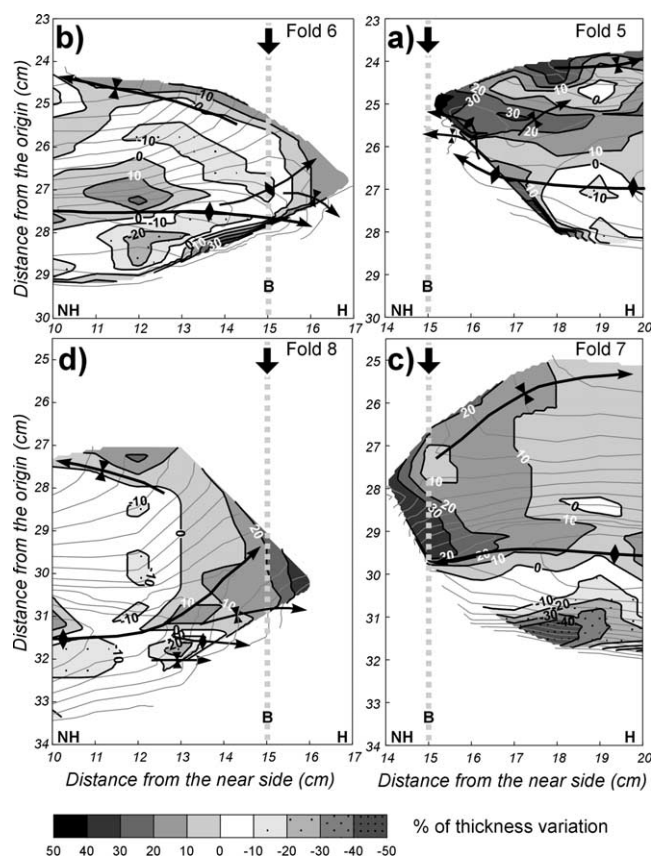
Fig. 13. Contouring of the percentage of layer L5 thickness changes for each pericline. (a) 5, (b) 6, (c) 7 and (d) 8. The greyscale refers to increase in thickness, and the symbols scale refers to decrease in thickness (contour interval 10%). The contour interval of folds (in grey) is 0.1 cm. Vertical grey dotted lines represent the boundary (B) between the non-homogeneous (NH) and the homogeneous (H) domains.

show an increase in the amount of faulting and a decrease in folding, yet the pattern of the curves remained the same. Despite the imperfections in the method, what we wished to emphasize was not an absolute amount of partitioned strain, but the relative difference between the two domains.

In the zone where the thrust fronts are oblique, some out-of-plane motion took place, as displayed by the distortion of the white grid at the topographic surface (Figs. 2 and 3). Nevertheless, the amount of slip loss, nearly 41% with respect to the adjacent 'normal' area, is too high to be explained by out-of-plane motion only. The strain partitioning analysis shows that (Fig. 12b):

- far from the boundary line, faulting accounts for 50–60% of shortening and is greater in the homogeneous domain than in the non-homogeneous;
- layer-parallel shortening is 30–40% and is slightly greater in the non-homogeneous domain;
- folding is relatively low, but is also greater in the non-homogeneous domain because of the strength contrast (Erickson, 1996).

A comparison between deep and shallow structural levels

allows the following observations:

- faulting is greater at depth in the non-homogeneous domain and, conversely, is greater near the surface in the homogeneous domain;
- layer-parallel shortening is everywhere greater at deeper structural levels;
- folding in the non-homogeneous domain is greater at shallow structural levels, but no differences seem to exist in the homogeneous domain.

Finally, the curves seem to indicate that the transfer zone is more extensive in the non-homogeneous domain. The most important feature is that, laterally along strike and entering the transfer zone, imbricate thrusts tip out and are replaced by layer-parallel shortening. Layer-parallel shortening is the dominant mechanism of deformation along the boundary between the two domains. The distribution pattern of the three mechanisms along the sections away from the transfer zone, i.e. in the 'normal' area, exhibits some differences with respect to the outcomes of Mulugeta and Koyi (1987), as they found that layer-parallel shortening accounted for 41%, and imbricate faulting for 44%, of the final shortening.

In the bed length balancing method employed, shortening due to faulting is the only value directly measured on the sections: folding and layer-parallel shortening are calculated from other parameters. For this reason, we tried to evaluate the model deformation better by measuring a single layer thickness variation. We chose the shallow layer 5 (labelled L5 in Fig. 1b), which is made of glass microbeads in the non-homogeneous domain. Contours of the percentage thickness variation have been overlaid on fold structure maps, in which both thickening and thinning of beds is displayed (Fig. 13). The analysis of the plots reveals that thickening:

- in general, increases towards periclinal depressions (over oblique ramps);
- in detail, is greater in the homogeneous than in the non-homogeneous domain (Fig. 13a and c);
- locally, slightly affects thrust sheet footwalls.

Conversely, thinning:

- in general is more distributed in the non-homogeneous domain because the glass microbeads layer is probably affected by layer-parallel shear mechanisms (Fig. 13b and d);
- occurs in all the fold forelimbs of both domains because of the steep topographic slope.

Now, a question arises from these outcomes: is the layer-parallel shortening in the sand partitioned in volume loss and compaction (that in nature means porosity reduction, cleavage and stylolite formation) or is layer-parallel

shortening transferred in increased thickness of a layer, i.e. the volume remains constant? Experimental studies on the compaction of dry clean sands (Rutter and Wanten, 2000) show almost no volume loss or, at least, less than 5% (Nowak et al., 1998). Such experiments are usually performed at higher strain than those produced in a sandbox experiment and on confined samples, so the results can be considered really extreme. Lohrmann et al. (2003) found very little either positive or negative variations of thickness (volume change) of various sand samples in their shear tests at very low normal stress (comparable with sandbox experiments). The difference is a function of the preparation technique of the sample. Our sandbox models are more likely suitable to dilation instead of compaction, according the preparation technique we used.

Regarding direct measurements in sand models, Wilkerson et al. (1992) recorded thickness changes in sand layers due to pure shear. They claimed the area increase had "resulted from dilation accompanying frictional sliding between sand grains and probably bear no direct relation to dilation magnitude in real rocks". On the contrary, measurements of layer-parallel compaction performed by Koyi and Vendeville (2003) in sand wedges revealed an area loss ranging from 2 to 5.8% (as the basal dip of the box changes) ascribed to the reduction of porosity between the sand grains, which corresponds to a layer-parallel shortening ranging from 9.5 to 15%. They conclude the deformation is partitioned by both compaction and thickening.

Our measurements concerning area changes (performed on all sections in the transfer zone) resulted in a widespread increment of 4.6% on average, showing a moderate maximum in the transfer zone. The dilation can be ascribed to the disorder of the normal arrangement of sand grains due to the deformation and also to the presence of faults. In sand models faults are shear bands in which the normal arrangements of grains changes, resulting in a decrease of the bulk density (Colletta et al., 1991). This suggests that, where faults are more numerous (in the transfer zone), dilation is also greater. If any sand compaction locally occurred, it would not be possible to detect with this method. Such outcomes allow us to state that the calculated layer-parallel shortening is partitioned in layers that thicken variably from place to place; layer-parallel shortening accommodates greater displacement in the transfer zone (Fig. 13) and, along with dilation between sand grains, globally resulted in a volume increase. So, once again, it is worthwhile carefully considering the contribution of layer-parallel shortening and layer thickening when dealing with section balancing, and in particular in transfer zones where both parameters reach greatest values.

We did not evaluate out-of-plane movement in the accommodation zone, but we think it accounts for only a very small amount of deformation. Plotting of the values of ramp dip and strike in (Fig. 8) of Apotria et al. (1992) resulted in an out-of-transport calculated deflection plane of about 3°. A numerical approach by Strayer and Suppe (2002) demonstrates that, in their experimental conditions, out-of-plane displacement of material can occur but is very little, in particular "is an order of magnitude or two less than in-plane displacement".

In general, in the transfer zone, the cumulative slip of two overlapping faults is less than in the 'normal' area because part of the deformation is transferred from faulting (slip) to layer-parallel shortening. Because we did not observe any thrust front rotation during the kinematic evolution, we can state that no significant along-strike extension occurred to accommodate strain in the fold (Husson and Mugnier, 2003). We did not detect any tear faults, which in nature are reported to possibly account for the accommodation of displacement gradients along the strike of the structures (Mueller and Talling, 1997).

4.5. Comparison with previous work

Laterally variable mechanical stratigraphy produced by means of interbedded 'weak' analogue materials has been only tested by Corrado et al. (1998). They used a Newtonian silicon gum layer instead of a brittle one. They also simultaneously applied a lateral thickness variation and a vertical step in the basement. Therefore, more than a single parameter influenced their modelled transfer zones. Nevertheless, in map view it is possible to note that the interbedded Newtonian décollement resulted in a braided architecture of thrust fronts and a diachronous kinematics between the two compartments.

The general braided architecture of our transfer zone looks similar to fold and fault geometries reported by other authors and reproduced by means of different boundary conditions (sand thickness variations: Marshak and Wilkerson, 1992; Marshak et al., 1992; Calassou et al., 1993). There also appears to be a close similarity with a model by Cotton and Koyi (2000), in which two different basal detachments (frictional and ductile) were placed next to each other. There the transfer zone also corresponds to a structural domain separating two different styles of fold and thrust belts. In fact, the use of Newtonian analogue materials allows the development of counter regional thrusts, which never occur in brittle stratigraphies. Differently from other experimental set ups (e.g. Cotton and Koyi, 2000; Bahroudi and Koyi, 2003), our lateral heterogeneity did not allow tear faults to occur.

Surface contouring allowed a better geometrical description, showing that the dip of oblique ramps and frontal ramps are similar, and comparable with the outcome described by Calassou et al. (1993). In our experiment, we emphasized the results of the interaction between different fault surfaces and periclines in the transfer zone, resulting in the development of lateral sub-culminations of folds and convex upward fault surfaces never described before in experimental literature.

The alternate thrust propagation on both sides of the transfer zone closely resemble the kinematics resulting from

lateral variation of backstop geometry and described by Calassou et al. (1993). More generally, the diachronous kinematic development has been observed in all the experiments characterized by any kind of lateral heterogeneities (both initial and sin-deformational) and braided architectures of thrusts.

The along-strike strain partitioning analysis has been performed before only by Liu and Dixon (1991) and Dixon and Liu (1992) in centrifuge models. They analysed the partitioning of strain using a different technique than the one used above. Their results show that layer-parallel shortening is the main deformation mechanism at deep structural levels (63% of the shortening), whereas folding represents the principal mechanism at shallow levels (55% of the shortening). Displacement transfer occurs along strike, as the occurrence of pericline and en-échelon structures reveal, but the low measurement resolution probably did not allow the authors to relate layer-parallel shortening lateral variations to the transfer zones.

5. Conclusions

The model along-strike mechanical stratigraphy zonation strongly affected the experimental geometries and kinematics. The final transfer zone separates two mechanical domains being deformed, so that the following conclusions result:

1. The kinematic sequence indicates a discontinuous development of the deformation front, which propagates intermittently and differently across the homogeneous domain and the non-homogeneous domain.
2. The lateral mechanical anisotropy resulted in the formation of oblique ramps. At the surface, oblique ramps are connected to oblique thrust fronts. An oblique thrust front can be (a) the linking structural feature between two thrust fronts with different wavelengths or (b) the lateral termination of a thrust sheet.
3. Analysis of the fault displacement suggests a complicated displacement transfer across the model structures; approaching the transfer zone, where the pericline depressions occur, slip along the faults is substituted by more layer-parallel shortening, which becomes the greatest deformation mechanism in the transfer zone, whereas folding remains nearly stable.
4. A linear relationship between thrust sheet bed length and slip appears to exist in the model structures. This relationship can help to predict the three-dimensional attributes of an emplaced thrust sheet. In addition, it may give some insights on the activity of a thrust sheet with respect to others of the same belt.
5. Detailed measurements of layer thicknesses reveal an increment towards the transfer zone. A decrease in layer thickness (i.e. tectonic thinning) particularly occurs in the forelimbs of the model folds.

The performed analogue model clearly reveals the different features that might occur across a compressional type, fold-fault related transfer zone. The resulting deformation fabric provides a three-dimensional overview of the possible architecture complexity arising within such a structure domain. The analysis of the continuous set of data across the experimental structures helps the quantitative evaluation of a transfer zone analogue to be performed. The real time evolution of the model transfer zone, observed on map view, suggests how deformation can progress within a thrust belt system as it attempts to link different structures, geometrically independent along-strike.

Application of the derived knowledge to natural transfer zone situations might be used to reduce the uncertainty in the reconstruction of the structure under evaluation. Eventually, the 'model' criteria presented or discussed by this study could represent alternative solutions to the interpretation of those geometries, which are partially exposed at surface or badly imaged at depth. As such, the model results could be a valid support in the prediction and prognosis of difficult targets, which might be suspected to occur in a transfer-zone contraction related structure setting.

References

Apotria, T.G., Snedden, W.T., Spang, J.H., Wiltschko, D.V., 1992. Kinematic models of deformation at an oblique ramp. In: McClay, K.R., (Ed.), Thrust Tectonics, Chapman and Hall, London, pp. 141–154.

Bahroudi, A., Koyi, H.A., 2003. Effect of spatial distribution of Hormutz salt on deformation style in the Zagros fold and thrust belt: an analogue modelling approach. Journal of the Geological Society of London 160, 719–733.

Barrier, L., Nalpas, T., Gapais, D., Proust, J.N., Casas, A., Bourquin, S., 2002. Influence of syntectonic sedimentation on thrust geometry. Field examples from the Iberian Chain (Spain) and analogue modeling. Sedimentary Geology 146, 91–104.

Blay, P., Cosgrove, J.W., Summers, J.M., 1977. An experimental investigation of the development of structures in multilayers under the influence of gravity. Journal of Geological Society of London 133, 329–342.

Burbank, D.W., McLean, J.K., Bullen, M., Abdrakhmatov, K.Y., Miller, M.M., 1999. Partitioning of intermontane basins by thrust-related folding, Tien Shan, Kyrgyzstan. Basin Research 11, 75–92.

Butler, R.W.H., 1992. Evolution of Alpine fold-thrust complexes: a linked kinematic approach. In: Mitra, S., Fisher, G. (Eds.), Structural Geology of Fold and Thrust Belts, The Johns Hopkins University Press, Baltimore, pp. 29–44.

Calassou, S., Larroque, C., Malavieille, J., 1993. Transfer zones of

deformation in thrust wedges: an experimental study. Tectonophysics 221, 325–344.

Cobbold, P.R., Castro, L., 1999. Fluid pressure and effective stress in sandbox models. Tectonophysics 301, 1–19.

Colletta, B., Letouzey, J., Pinedo, R., Ballard, J.F., Balé, P., 1991. Computerized X-ray tomography analysis of sandbox models: examples of thin-skinned thrust systems. Geology 19, 1063–1067.

Corrado, S., Di Bucci, D., Naso, G., Faccenna, C., 1998. Influence of palaeogeography on thrust system geometries: an analogue modelling approach for the Abruzzi–Molise (Italy) case history. Tectonophysics 296, 437–453.

Cotton, J.T., Koyi, H.A., 2000. Modeling of thrust fronts above ductile and frictional detachments: application to structures in the Salt Range and Potwar Plateau, Pakistan. Geological Society of America Bulletin 112, 351–363.

Coward, M.P., Potts, G.J., 1983. Complex strain patterns developed at the frontal and lateral tips to shear zones and thrust zones. Journal of Structural Geology 5, 383–399.

Dahlstrom, C.D.A., 1970. Structural geology of the eastern margin of the Canadian Rocky Mountains. Bulletin of Canadian Petroleum Geology 18, 332–406.

Davis, D., Suppe, J., Dahlen, F.A., 1983. Mechanics of fold-and-thrust belts and accretionary wedges. Journal of Geophysical Research 94, 10347–10354.

Dixon, J.M., Liu, S., 1992. Centrifuge modelling of the propagation of thrust faults. In: McClay, K.R., (Ed.), Thrust Tectonics, Chapman and Hall, London, pp. 53–69.

Erickson, S.G., 1996. Influence of mechanical stratigraphy on folding vs faulting. Journal of Structural Geology 18, 443–450.

Fischer, M.P., Woodward, N.B., 1992. The geometric evolution of foreland thrust systems. In: McClay, K.R., (Ed.), Thrust Tectonics, Chapman and Hall, London, pp. 181–189.

Geiser, P.A., 1988. Mechanisms of thrust propagation: some examples and implications for the analysis of overthrust terranes. Journal of Structural Geology 10, 829–845.

Gomes, C.J.S., Pereira Filho, M., Braga, S.C.M., 2003. Experimental models of 'Basement'-controlled salients—application to the Proterozoic fold-thrust belt of the Quadrilátero Ferrífero (Minas Gerais, Southeastern Brasil). Anais da Academia Brasileira de Ciências 75, 249–263.

Husson, L., Mugnier, J.-L., 2003. Three-dimensional horizon reconstruction from outcrop structural data, restoration, and strain field of the Baisahi anticline, Western Nepal. Journal of Structural Geology 25, 79–90.

Koyi, H.A., 1995. Mode of internal deformation in sand wedges. Journal of Structural Geology 17, 293–300.

Koyi, H.A., 1997. Analogue modelling: from a qualitative to a quantitative technique—a historical outline. Journal of Petroleum Geology 20, 223–238.

Koyi, H.A., Vendeville, B.C., 2003. The effect of décollement dip on geometry and kinematics of model accretionary wedges. Journal of Structural Geology 25, 1445–1450.

Letouzey, J., Colletta, B., Vially, R., Chermette, J.C., 1995. Evolution of salt-related structures in compressional settings. In: Jackson, M.P.A., Roberts, D.G., Snelson, S. (Eds.), Salt Tectonics: a Global Perspective, American Association of Petroleum Geologists Memoir, 65, pp. 41–60.

Lickorish, W.H., Ford, M., Bürgisser, J., Cobbold, P.R., 2002. Arcuate thrust systems in sandbox experiments: a comparison to the external arcs of the Western Alps. Geological Society of America Bulletin 114, 1089–1107.

Liu, S., Dixon, J.M., 1991. Centrifuge modelling of thrust faulting: structural variation along strike in fold-thrust belts. Tectonophysics 188, 39–62.

Liu, H., McClay, K.R., Powell, D., 1992. Physical models of thrust wedges. In: McClay, K.R., (Ed.), Thrust Tectonics, Chapman and Hall, London, pp. 71–81.

Lohrmann, J., Kukowski, N., Adam, J., Oncken, O., 2003. The impact of analogue material properties on the geometry, kinematics, and dynamics of convergent sand wedges. Journal of Structural Geology 25, 1691–1711.

Luián, M., Storti, F., Balanyá, J.C., Crespo-Blanc, A., Rossetti, F., 2003. Role of décollement material with different rheological properties in the structure of the Aljibe thrust imbricate (Flysch Trough, Gibraltar Arc): an analogue modelling approach. Journal of Structural Geology 25, 867–881.

Marques, F.O., Cobbold, P.R., 2002. Topography as a major factor in the development of Arcuate thrust belts: insights from sandbox experiments. Tectonophysics 348, 247–268.

Marshak, S., Wilkerson, M.S., 1992. Effect of overburden thickness on thrust belt geometry and development. Tectonics 11, 560–566.

Marshak, S., Wilkerson, M.S., Hsui, A.T., 1992. Generation of curved fold-thrust belts: insight from simple physical and analytical models. In: McClay, K.R., (Ed.), Thrust Tectonics, Chapman and Hall, London, pp. 83–92.

Mueller, K., Talling, P., 1997. Geomorphic evidence for tear faults accommodating lateral propagation of an active fault-bend fold, Wheeler Ridge, California. Journal of Structural Geology 19, 397–411.

Mulugeta, G., Koyi, H.A., 1987. Three-dimensional geometry and kinematics of experimental piggyback thrusting. Geology 15, 1052–1056.

Mulugeta, G., Koyi, H.A., 1992. Episodic accretion and strain partitioning in a model sand wedge. Tectonophysics 202, 319–333.

Needham, D.T., Yielding, G., Freeman, B., 1996. Analysis of fault geometry and displacement patterns. In: Buchanan, P.G., Nieuwland, D.A. (Eds.), Modern Developments in Structural Interpretation, Validation and Modelling, Geological Society Special Publication, 99, pp. 189–199.

Nicol, A., Gillespie, P.A., Childs, C., Walsh, J.J., 2002. Relay zones between mesoscopic thrust faults in layered sedimentary sequences. Journal of Structural Geology 24, 709–727.

Nowak, E.R., James, B., Knight, J.B., Eli Ben-Naim, E.B., Jaeger, H.M., Nagel, S.R., 1998. Density fluctuations in vibrated granular materials. Physical Review E 57, 1971–1982.

Philippe, Y., Deville, E., Mascle, A., 1998. Thin-skinned inversion tectonics at oblique basin margins: example of the western Vercors and Chartreuse Subalpine massifs (SE France). In: Mascle, A., Piugdefàbregas, C., Luterbacher, H.P., Fernàndez, M. (Eds.), Cenozoic Foreland Basins of Western Europe, Geological Society Special Publication, 134, pp. 239–262.

Ranalli, G., 2001. Experimental tectonics: from Sir James Hall to the present. Journal of Geodynamics 32, 65–76.

Rowan, M.G., 1997. Three-dimensional geometry and evolution of a segmented detachment fold, Mississippi Fan foldbelt, Gulf of Mexico. Journal of Structural Geology 19, 463–480.

Rutter, E.H., Wanten, P.H., 2000. Experimental study of the compaction of phyllosilicate-bearing sand at elevated temperature and with controlled pore water pressure. Journal of Sedimentary Research 70, 107–116.

Sassi, W., Colletta, B., Balé, P., Paquereau, T., 1993. Modelling of structural complexity in sedimentary basins: the role of pre-existing faults in thrust tectonics. Tectonophysics 226, 97–112.

Schellart, W.P., 2000. Shear test results for cohesion and friction coefficients for different granular materials: scaling implications for their usage in analogue modelling. Tectonophysics 324, 1–16.

Schellart, W.P., 2002. Analogue modelling of large-scale tectonic processes: an introduction. In: Schellart, W.P., Passchier, C. (Eds.), Analogue Modelling of Large-Scale Tectonic Processes, Journal of the Virtual Explorer, 7, pp. 1–6.

Schreurs, G., Hänni, R., Vock, P., 2001. Four-dimensional analysis of analog models: experiments on transfer zones in fold and thrust belts. In: Koyi, H.A., Mancktelow, N.S. (Eds.), Tectonic Modeling: A Volume in Honor of Hans Ramberg, Geological Society of America Memoir, 193, pp. 179–190.

Soto, R., Casas, A.M., Storti, F., Faccenna, C., 2002. Role of lateral thickness variations on the development of oblique structures at the

Western end of the South Pyrenean Central Unit. Tectonophysics 350, 215–235.

Soto, R., Storti, F., Casas, A.M., Faccenna, C., 2003. Influence of along-strike pre-orogenic sedimentary tapering on the internal architecture of experimental thrust wedges. Geological Magazine 140, 253–264.

Strayer, L.M., Suppe, J., 2002. Out-of-plane motion of a thrust sheet during along-strike propagation of a thrust ramp: a distinct-element approach. Journal of Structural Geology 24, 637–650.

Thomas, W.A., Bayona, G., 2002. Palinspastic restoration of the Anniston transverse zone in the Appalachian thrust belt, Alabama. Journal of Structural Geology 24, 797–826.

Turrini, C., Ravaglia, A., Perotti, C.R., 2001. Compressional structures in a multilayered mechanical stratigraphy: insights from sandbox modeling with three-dimensional variations in basal geometry and friction. In: Koyi, H.A., Mancktelow, N.S. (Eds.), Tectonic Modeling: A Volume in Honor of Hans Ramberg, Geological Society of America Memoir, 193, pp. 153–178.

Wilkerson, M.S., Marshak, S., Bosworth, W., 1992. Computerized tomographic analysis of displacement trajectories and three-dimensional fold geometry above oblique thrust ramps. Geology 20, 439–442.

Wilkerson, M.S., Apotria, T., Farid, T., 2002. Interpreting the geologic map expression of contractional fault-related fold terminations: lateral/oblique ramps versus displacement gradients. Journal of Structural Geology 24, 593–607.